ACS APPLIED MATERIALS & INTERFACES

Research Article

www.acsami.org

One-Step In situ Synthesis of SnO_2/Graphene Nanocomposites and Its Application As an Anode Material for Li-Ion Batteries

Junfei Liang, Wei Wei, Da Zhong, Qinglin Yang, Lidong Li,* and Lin Guo*

Key Laboratory of Bio-Inspired Smart Interfacial Science and Technology of Ministry of Education, School of Chemistry and Environment, Beijing University of Aeronautics & Astronautics, Beijing, 100191, P. R. of China

ABSTRACT: A facile one-step solution-based process to in situ synthesize SnO_2/graphene (SG) nanocomposites was developed, by using the mixture of dimethyl sulfoxide (DMSO) and H_2O as both solvent and reactant. The reduction of graphene oxide (GO) and the in situ formation of SnO_2 nanoparticles were realized in one step. The electrochemical experiments showed the composites provided a better Li-storage performance. The method presented in this paper may provide an effective, economic, and green strategy for the preparation of metal-oxide/graphene nanocomposites.

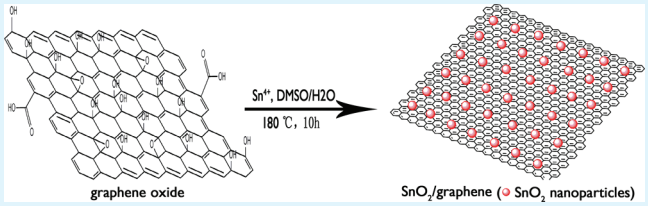

KEYWORDS: *SnO_2, graphene, nanocomposites, solution processes, one-step, in situ, Li-ion battery*

1. INTRODUCTION

Modern electronic devices such as mobile communication devices, portable electronic devices, and electric/hybrid vehicles require high-performance batteries to power them.[1] Li-ion battery is one of the most suitable candidates to satisfy the requirements because of its high energy density, high voltage, and light weight. In the case of a battery, electrode material is a determining factor for the battery performance.[2−5] Although graphite performs well as anode for commercial Li-ion batteries (LIBs), its theoretical capacity is insufficient to satisfy the increasing demand for batteries with higher capacity. For the purpose of improving the energy density of LIBs, scientists have made great efforts to explore alternative anode materials with higher capacity. Many materials including metal oxide, metal sulfide, and nonmetal with large specific capacity have been studied to replace graphite.[1,3,6] Among these materials, SnO_2 has attracted much attention because of its high theoretical reversible Li^+ storage capacity (calculated to be 782 mA h g^{-1}), which is much larger than the theoretical capacity of currently used graphite (372 mA h g^{-1}).[7] However, the practical application of SnO_2 as anode is hampered by its poor cycle performance, resulting from the serious volume expansion and contraction (up to about 300%) during the insertion and extraction processes of Li^+.[8,9] To address this problem, various methods have been tested.[8−17] Results have shown that hybridizing SnO_2 with carbon materials is an effective method to accommodate the strain of volume change during the charge/discharge process.[16−20]

Graphene, a single-atom-thick sheet of honeycomb carbon lattice, exhibits a number of intriguing properties, such as high specific surface area, excellent conductivity and good mechanical flexibility.[21−23] The superior electronic conductivity and mechanical properties of graphene make it suitable for fabrication into high-performance composites with other anode materials for LIBs. Graphene is generally prepared by chemical oxidation of graphite to exfoliated sheets of GO, followed by reduction with highly toxic hydrazine or sodium borohydride.[24,25] However, a serious problem is that the reduced graphene oxide sheets (RGOs) are not stable in solution and tend to aggregate,[26,27] therefore lose its unique properties. By incorporation of nanoparticles into RGOs, because of the good distribution of nanoparticles, the aggregation problem of RGOs could be minimized or prevented.[28]

In the past several years, solution processes have become noteworthy as an important nanofabrication technique of functional materials.[29] To date, there have been a few reports of the preparation of SG nanocomposites in a solution system. However, these processes are usually complicated and time-consuming, involving a multistep approach resulting in the inhomogeneous dispersion of nanoparticels on the graphene matrix,[30−34] or use of additional chemicals such as ethylene glycol or sodium borohydride, which are either hygroscopic or toxic.[35,36] Therefore, it is still necessary to explore an efficient, economic, and green method for the synthesis of SG nanocomposites. Different from some reported methods to prepare the nanocomposites of SG based on oxidation−reduction reaction between GO and Sn^{2+},[37−41] we developed a facile one-step solution route to in situ chemically synthetize SG nanocomposites from GO, DMSO/H_2O and Sn^{4+} for the first time. The mixture of DMSO and H_2O was used as both solvent and reactant. In the reaction system, DMSO not only reduces GO to RGOs, but also results in the formation of SnO_2 nanoparticles facilitated by the presence of H_2O. The advantages of this work are characterized by a facile one-step procedure, that is, the reduction of GO and the deposition of SnO_2 nanopaticles on RGOs occur simultaneously, an extra

Received: November 4, 2011
Accepted: December 21, 2011
Published: December 21, 2011

Scheme 1. Scheme Illustration for the Synthesis of SG Nanocomposites

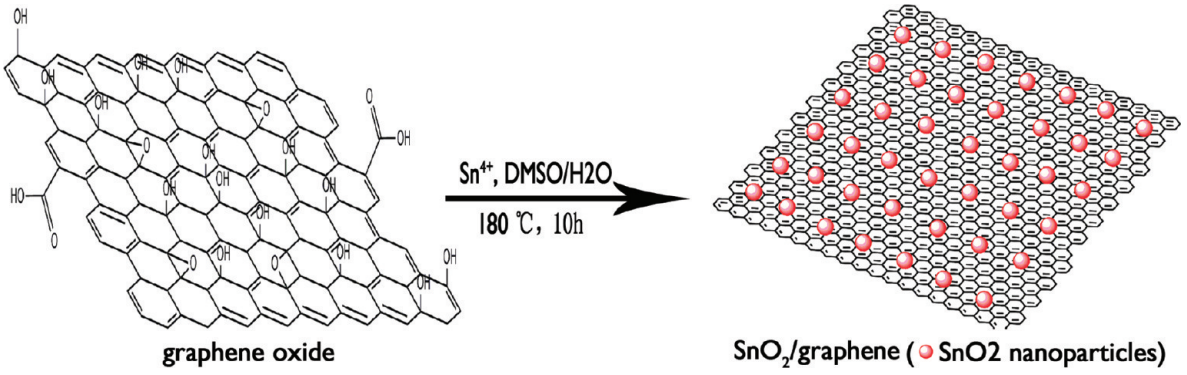

reducing agent such as toxic sodium borohydride is not required for the reduction of GO to RGOs in our procedure. The in situ growth of metal oxides leads to the formation of uniform nanoparticles on RGOs, SnO_2-decoration helps to prevent not only the aggregation of the RGOs, but also the aggregation of SnO_2 nanopaticles. Enhanced electrochemical performance of the as synthesized nanocomposites as an anode material in LIBs was obtained.

2. EXPERIMENTAL SECTION

2.1. Chemical Reagents and Materials. Graphite powder (325 mesh, with purity >99.99%) was obtained from Alfa Aesar. All other chemicals (purchased from Beijing Chemical Co.,Ltd.) used in this experiment were analytical grade and were used without further purification.

2.2. Preparation of SG Nanocomposites. GO was synthesized from natural graphite powder by a modified Hummer's method as originally presented by Kovtyukhova et al.[42] GO was then subjected to dialysis for 7 days to completely remove metal ions and acids. Finally, the product was dried in air at room temperature. In a typical synthesis of the nanocomposites, 100 mg GO was dispersed in the mixture (100 mL) of DMSO and H_2O with the volume ratio of DMSO/H_2O = 9:1by sonication for 1.5 h, forming a stable GO suspension. Afterward, 1 g of $SnCl_4.5H_2O$ was added into the resulting homogeneous dispersion. After 30 min of ultrasonic treatment, the mixture was refluxed at 180 °C for 10 h, resulting in a black suspension. At the end, the as-synthesized product was collected by centrifugation, which was then rinsed with absolute ethanol 6 times. Finally, the product was dried in air at room temperature for further characterization. In order to improve the crystallinity of SnO_2 in the composites, the product was annealed at 400 °C for 2 h in Ar atmosphere.

2.3. Characterizations. The structures and compositions of the as-prepared products were characterized by X-ray powder diffraction (XRD) using a Rigaku Dmax 2200 X-ray diffractometer with Cu Kα radiation (λ = 1.5416 Å). The XRD specimens were prepared by means of flattening the powder on the small slides. Transmission electron microscopy (TEM) and high-resolution TEM (HRTEM) investigations were carried out by a JEOL JEM-2100F microscope. The as-prepared samples were dispersed in ethanol and dropped onto a carbon film supported on a copper grid for the drying process in air. Raman spectrometer was recorded on a LabRAM HR800(HORIBA Jobin Yvon) confocal Raman spectrometer, with an excitation laser wavelength of 514.5 nm. All samples were deposited on silicon wafers in powder form without using any solvent. Thermogravimetric analysis (TGA) was performed in air using a Pyris Diamond TG/DTA (PerkinElemer Inc., U.S.A). The samples were heated from 50 to 700 °C at 10 °C/min.

2.4. Electrochemical Measurements. The electrochemical properties of the SG nanocomposites and commercial SnO_2 nanocrystals as anode materials in lithium ion cells were evaluated by galvanostatic charge/discharge technique. The test electrodes were prepared by mixing 80 wt % active material with 10 wt % carbon black and 10 wt % polyvinylidene fluoride (PVDF) dissolved in N-methyl-2-pyrrolidone (NMP) to form a slurry, which was then coated onto a copper foil (current collector), dried at 80 °C for 10 h and finally pressed under pressure of 10 MPa. Afterward, CR2016 type coin cells were assembled in an highly pure argon-filled glovebox using the test electrodes, the metallic lithium counter/reference electrode, a polypropylene separator (Celgard 2400), an electrolyte of 1 mol/L $LiPF_6$ in ethylene carbonate and diethyl carbonate (EC/DMC, 1:1 vol) (Tianjin Jinniu Power Sources Material Co., Ltd. China). Charge−discharge measurements were carried out galvanostatically at a current density of 100 mA g^{-1} in the voltage range of 0.005−1.5 V using a battery test system (LAND CT2001A model, Wuhan Jinnuo Electronics. Ltd., China). The electrochemical impedance measurements were performed on CHI660D electrochemical workstation (Shanghai Chenhua Co. Ltd., China) at an AC voltage of 5 mV amplitude in the 100 kHz to 0.01 Hz.

3. RESULTS AND DISCUSSION

In this work, we adopted a convenient in situ method to fabricate RGOs decorated with SnO_2 nanoparticles. The overall procedure is illustrated in Scheme 1. Previous studies have indicated that the GO nanosheets have their basal planes decorated mostly with epoxy and hydroxyl groups, in addition to carboxyl groups located presumably at the edges.[43] First, the GO was dispersed in DMSO/H_2O to form a uniform GO nanosheets suspension by sonication because of these oxygenate species. When GO solution was mixed with $SnCl_4{\cdot}5H_2O$ solution, the Sn^{4+} was selectively bonded with the oxygenated groups by electrostatic force.[44] After refluxed at 180 °C for 10 h, the GO nanosheets were reduced to RGOs and the anchored Sn^{4+} ions were converted to SnO_2 nanoparticles. The reduction mechanism of GO in this process may be a result of thermal reduction and the production of the reductant H_2S from DMSO at 180 °C.[28] The possible formation mechanism of SnO_2 nanopaticles can be described by the following reactions

$$Sn^{4+} + 4H_2O \leftrightarrow Sn(OH)_4 + 8H^+ \quad (1)$$

$$Sn(OH)_4 \xrightarrow[\text{dehydration}]{\text{reflux}} SnO_2 + 2H_2O \quad (2)$$

H_2S generated during the decomposition of DMSO could neutralize H^+ produced by reaction 1, which helped to produce a relatively high concentration of $Sn(OH)_4$ nuclei on RGOs. The $Sn(OH)_4$ nuclei were not stable in ambilence as observed previously. At a high temperature (180 °C), the $Sn(OH)_4$ nucleus should be converted to small SnO_2 nanopaticles. Our process can ensure the in situ formation of SnO_2 nanoparticles uniformly and reduction of GO to RGOs simultaneously, with

dx.doi.org/10.1021/am201541s | ACS Appl. Mater. Interfaces 2012, 4, 454−459

advantages of alleviating any serious stacking of RGOs sheets and preventing the agglomeration of SnO_2 nanoparticles.

The representative XRD pattern of GO and SG nanocomposites are shown in Figure 1. The peak at 10.4° in curve a

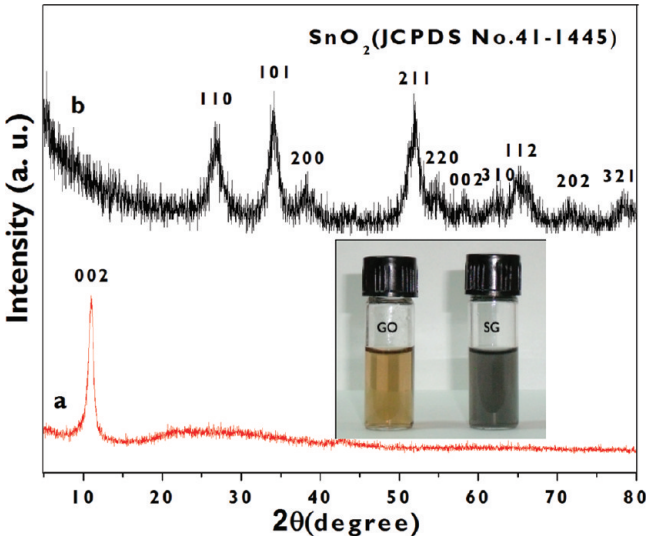

Figure 1. XRD patterns of (a) GO and (b) SG; the inset is the photograph of the GO and SG solution.

is characteristic for GO with an interlayer spacing of 0.85 nm, resulting in facile exfoliation due to the weakened van der Waals forces between layers of GO.[38] For samples of SG, no diffraction peaks of layered GO can be observed, indicating the absence of layer-stacking regularity after the reduction of GO.[39] The photograph of the GO and SG solution are shown in the inset of Figure 1. The color of the suspension shifts from brown (GO) to black (SG) during the reaction, which further confirms the successful reduction of GO. No obvious diffraction peak assigned to RGOs was found in the XRD pattern of the nanocomposites, because most RGOs were separated by nanoparticles, SnO_2 nanoparticles can interact with the RGOs through physisorption, electrostatic binding or charge transfer interactions.[37] By incorporation of nanoparticles into RGOs, the aggregation problem of RGOs could be minimized or prevented, favoring the maintenance of high surface area and other intrinsic chemical and physical properties of graphene.[45]

Raman spectroscopy is a powerful tool to characterize carbonaceous materials. The significant structural changes occurring during the chemical processing from GO to SG are reflected in their Raman spectra (Figure 2). The Raman spectrum of GO contains G band at 1594.6 cm^{-1} (E_{2g} phonon of C sp^2 atoms), owing to the presence of isolated double bonds that resonate at higher frequencies than the G band of graphite. Compared with graphite, the D band(1363.9 cm^{-1}, κ-point phonons of A_{1g} symmetry) of GO becomes evident, indicating the reduction in size of the in-plane sp^2 domains due to the extensive oxidation.[38,46] Both G band and D band can be also observed in the Raman spectra of SG nanocomposites, however, with an increased D/G intensity ratio compared to that in GO. This change suggests a decrease in the average size of the sp^2 domains upon reduction of the exfoliated GO, and can be explained if new graphitic domains were created that are smaller in size to the ones present in GO before reduction, but more numerous in number. A 2D band, which is the

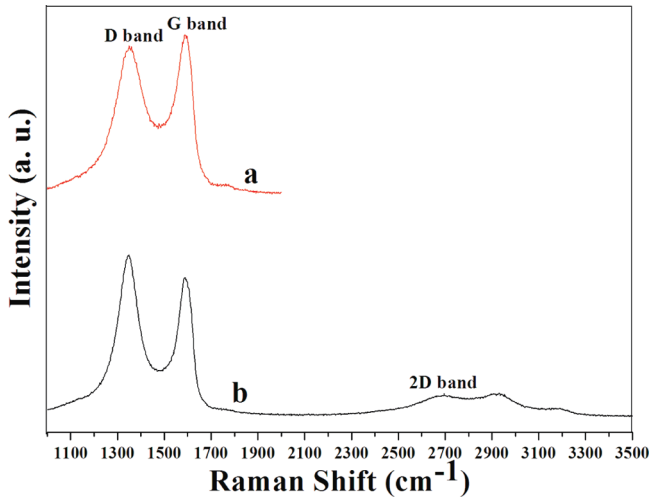

Figure 2. Raman spectra of (a) GO and (b) the SG.

characteristic band of graphene, is usually used to determine the number of layers of graphene in the sample. This band originated from a two-phonon double-resonance Raman process associated with the band structure of graphene. A 2D band observed in Figure 2 in different regions indicates that the composite has 2−5 layers of graphene.[16] Liu et al reported that the electrical conductivity of DMSO-reduced RGOs was comparable to or slightly better than that of the hydrazine-reduced RGOs which was about 5 orders of magnitude better than the conductivity of GO and very close to approaches that of pristine graphite.[24,28]As a result, the SnO_2/graphene composites are suitable for Li-ion batteries because of the excellent conductivity of RGOs.

The crystalline structure of the SG nanocomposites were analyzed by TEM and HRTEM. Figure 3a shows a low magnification TEM image of the SG nanocomposites, worm-like SnO_2 nanoparticles are uniformly distributed on the surface of RGOs. A HRTEM image of the SG nanocomposites is shown in Figure 3b, showing the average particle size of the SnO_2 is less than 8 nm. The lattice-resolved image of SG shows a lattice spacing of 0.33 nm and 0.26 nm, corresponding to the *d*-spacing of (110) and (101) crystal planes of SnO_2, respectively. The stacking of graphene nanosheets amounts of 3−5 layers, which can be counted from the number of strips as marked with arrows in Figure 3c), the results is consistent with the results from the Raman characterization. This structure, nanoparticles scattered on flexible RGOs, which can preserve the 3-dimensional structure of the SG nanocomposite, may be beneficial for the electron transfer and accommodation of the strains of Li^+ insertion/extraction, resulting in excellent Li^+ storage properties.[40]

To quantify the mass percentage of SnO_2, the as-prepared composites were analyzed by TGA. As shown in the TGA curves (Figure 4), the SG nanocomposite shows a rapid mass loss between 400 and 650 °C due to the oxidation of RGOs. Therefore, according to the change of weight, it is estimated that the amount of SnO_2 in the nanocomposite is 74%.

The SG nanocomposites with highly dispersed SnO_2 nanocrystals, high SnO_2 content, and excellent conductive graphene layer are desirable features for electrode materials in LIBs. To investigate the electrochemical performance of the SG nanocomposite as an anode for LIBs, discharge/charge cycling was carried out in the voltage range of 0.005−1.5 V (vs Li/Li^+)

dx.doi.org/10.1021/am201541s | ACS Appl. Mater. Interfaces 2012, 4, 454−459

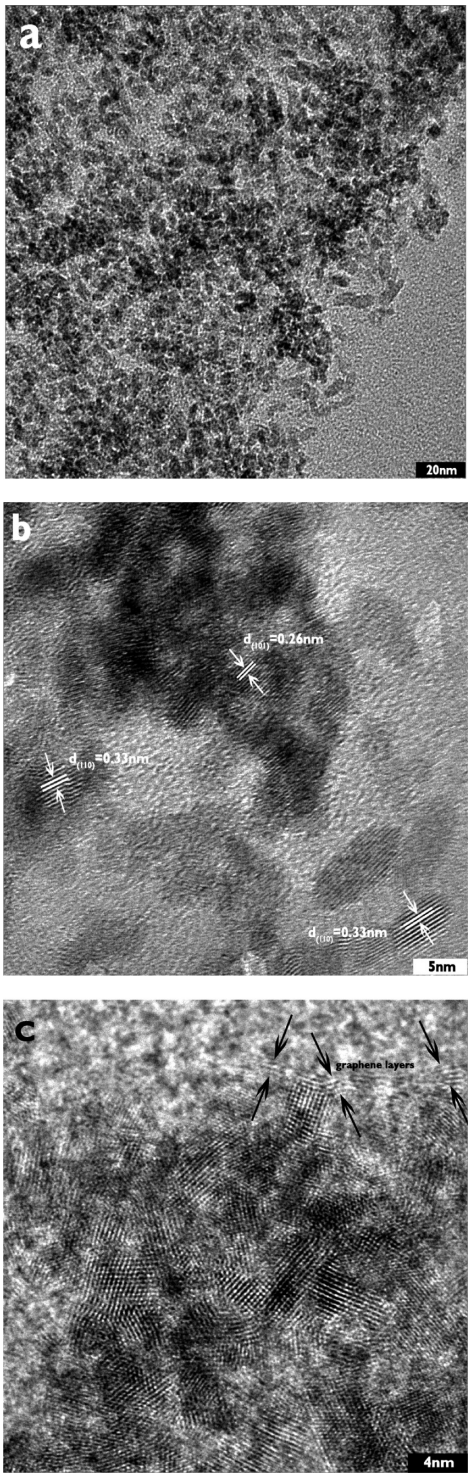

Figure 3. (a) TEM and (b,c) HRTEM image of the SG nanocomposites.

at a current density of 100 mA g^{-1} under room temperature. For comparison, commercial SnO_2 nanocrystals were also tested. Figure 5a shows the typical charge/discharge profiles of the nanocomposite in the second, fifth, and tenth cycles. The shape of the profiles did not change significantly during cycling, indicating the good stability of the nanocomposite as an anode. In general, SnO_2-based anode shows classical plateaus around 0.8 V similar to that of a bulk SnO_2 system, which has been well-known as the reaction of SnO_2 with lithium to form the

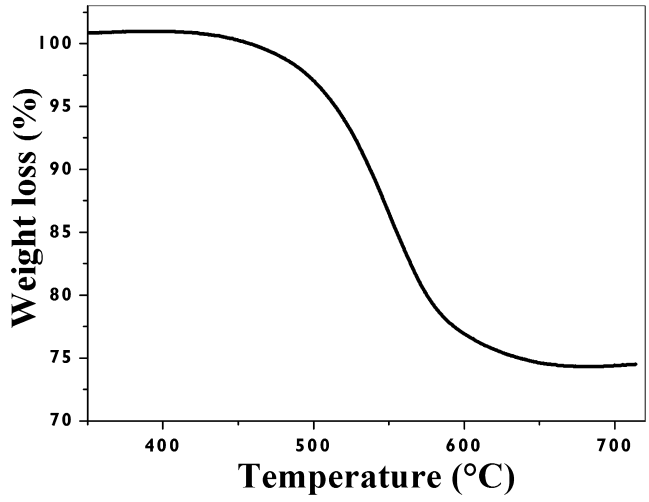

Figure 4. TGA curves of the SG nanocomposites.

solid electrolyte interface (SEI) layers. However, in case of the SG, this plateau around 0.8 V nearly disappeared after the first cycle, indicating that Li_2O is formed only in small quantities as a result of small particle size of SnO_2 in this nanocomposite. Such a result is related to the enhanced surface electrochemical reactivity due to the large surface-to-volume ratio.[30]

Figure 5b shows the cyclic performances of SG nanocomposite and commercial SnO_2 nanocrystals. For SG nanocomposite electrode, the discharge capacity dropped rapidly in the first cycle due to formation of amorphous Li_2O matrix and intense surface reactions with the Li−Sn compounds and the electrolyte solution.[35] In the subsequent charge/discharge cycles, Li^+ were reversibly inserted into Sn as LixSn alloys. From the second cycle, the SG anode showed highly reversible behavior. The SG nanocomposites exhibited a reversible capacity of 690 mA h g^{-1}. Furthermore, their cycling performanceis was drastically enhanced, as shown in the Figure 5b. After 20 cycles,the charge capacity still remained 433 mA h g^{-1}, which is about 63% retention of the reversible capacity, which is higher than other SG composites.[38] This performance is a little worse than the results reported previously;[30,35] however, the charge and discharge was carried out in a current density of 100 mA hg^{-1}, which is higher than the current density of 50 and 55 mA h g^{-1} used in these references. On the other hand, the commercial SnO_2 nanocrystals electrode exhibited a poor cycle performance, there was a rapid fading of capacity due to the severe pulverization, fading rapidly from 602 to 172 mA hg^{-1} after 20 cycles with about 29% retention of the reversible capacity. Compared with the commercial SnO_2 nanocrystals the SG nanocomposite exhibited superior charge capacity and cycling performance. In order to clarify the influence of the hybridization on the electrochemical performance of SG, the theoretical capacity of SG nanocomposite was estimated by calculating the capacity of physical mixture of pristine materials (SnO_2 and graphene) according to the theoretical capacities of the SnO_2 (782 mA h g^{-1})and graphene (744 mA h g^{-1}). On the basis of the weight content (74 wt % SnO_2 and 26 wt % graphene) determined by TGA, the theoretical capacity of SG nanocomposite was calculated to be 675.4 mA h g^{-1}. Despite the considerable drop, the charge capacity of SnO_2/graphene nanocomposite still remains 64.1% of the theoretical value after 20 cycles. As mentioned before, the main reason for a rapidfading of SnO_2 electrode is that a

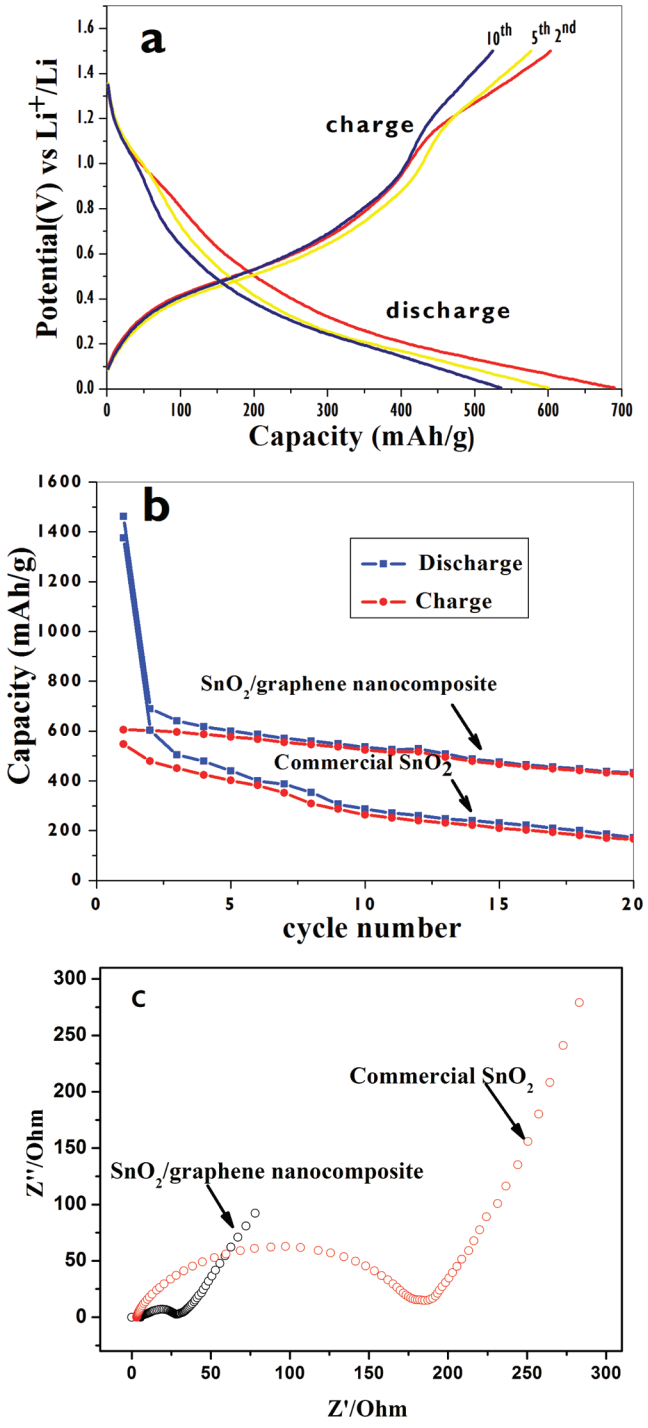

Figure 5. (a) Charge/discharge profile for SG, (b) the cycle performance of SG and commercial SnO_2 nanocrystals, (c) Nyquist plots of SG and commercial SnO_2 nanocrystals obtained by applying a sine wave with amplitude of 5.0 mV over the frequency range from 100 kHz to 0.01 Hz.

large volume expansion of the SnO_2 occurs during the charge–discharge cycle, leading tocracking and pulverization of the electrode. The commercial SnO_2 nanoparticles have a poor cycle performance, the improved performance observed in our experiments should be attributed to the combination of SnO_2 and RGOs. The RGOs with high surface area can help to build a better conductive network which could promote the electron transfer during the lithiation and delithiation process, the close contact between the SnO_2 nanoparticles and the RGOs can minimize the electrical isolation of nanoparticles during battery cycles. On the other hand, the high mechanical flexibility of RGOs might virtually work as a barrier to avoid the aggregation of SnO_2 nanoparticles and also as a buffer to prevent the volume expansion and contraction of SnO_2 nanoparticles during Li^+ insertion/extraction.

To verify the good electrochemical performance of composite in comparison with pure metal oxide particle, AC impedance spectra measurements were carried out. Figure 5c shows AC impedance spectra of the sample electrodes measured at the open potential of 0.8 V. The impedance spectra of the commercial SnO_2 nanocrystals and SG nanocomposites electrodes were obtained in the fifth discharge cycle. The high-frequency semicircle is attributed to SEI film resistance, and the spectra in the medium frequency include features that are usually semicircular in shape and related to charge transfer resistance.[47] From Figure 5c, the diameter of the semicircle for the composites electrode in the high–medium frequency region is much smaller than that of pure commercial SnO_2 electrode, which indicates that the composite possess lower contact and charge-transfer resistances when the surface area of both samples is same in the measurement of the impedance. This result shows that graphene in the composites not only improve the high conductivity of the overall electrode, but also largely enhance the electrochemical activity of SnO_2 nanopaticles during the cycle processes.

4. CONCLUSION

In summary, we developed a facile one-pot solution-based process to in situ synthesize SG nanocomposites. The reduction of GO to RGOs and the in situ formation of SnO_2 nanopaticles were realized in one step, which provided a simple, low-cost, effective, and green way to prepare SG nanocomposites because no additional toxic chemicals were needed. The use of DMSO and H_2O mixture solution was critical for this reaction. DMSO was an effective reducing agent to reduce GO to RGOs at the high temperature. On the other hand, water was involved in the formation of tin hydroxide, which resulted in the formation of SnO_2 nanoparticles deposited on RGOs. SnO_2-decoration on RGOs can prevent not only the aggregation of the RGOs but also the aggregation of SnO_2 nanoparticles. The electrochemical results show the composites provide a better Li-storage performance. When considering the plentiful properties for both SnO_2 and graphene,the composites could be promisingly applied in many research fields such as ultracapacitors, biosensor, gas sensor, gas storage, and electrochemical analysis in the future. Furthermore, this synthesis method may provide a facile, economic, and green strategy for the preparation of other metal-oxide/graphene nanocomposites.

AUTHOR INFORMATION

Corresponding Author

*Tel & Fax: +86-010-82338162. E-mail: lilidong@buaa.edu.cn (L.L.); guolin@buaa.edu.cn (L.G.).

ACKNOWLEDGMENTS

This project was financially supported by National Natural Science Foundation of China (11079002, 20903008, and 20973019) as well as by Specialized Research Fund for the

Doctoral Program of Higher Education (20091102110035 and 20111102130006).

REFERENCES

(1) Tarascon, J. M.; Armand, M. *Nature* **2001**, *414*, 359−367.
(2) Kang, K. S.; Meng, Y. S.; Breger, J.; Grey, C. P.; Ceder, G. *Science* **2006**, *311*, 977−980.
(3) Chan, C. K.; Peng, H. L.; Liu, G.; Mcllwrath, K.; Zhang, X. F.; Huggins, R. A.; Cui, Y. *Nat. Nanotechnol.* **2008**, *3*, 31−35.
(4) Etacheri, V.; Marom, R.; Elazari, R.; Salitra, G.; Aurbach, D. *Energy Environ. Sci.* **2011**, *4*, 3243−3262.
(5) Rao, C. V.; Reddy, A. L. M.; Ishikawa, Y.; Ajayan, P. M. *ACS Appl. Mater. Interfaces* **2011**, *3*, 2966−2972.
(6) Arico, A. S.; Bruce, P.; Scrosati, B.; Tarascon, J. M.; Van Schalkwijk, W. *Nat. Mater.* **2005**, *4*, 366−377.
(7) Idota, Y.; Kubota, T.; Matsufuji, A.; Maekawa, Y.; Miyasaka, T. *Science* **1997**, *276*, 1395−1397.
(8) Larcher, D.; Beattie, S.; Morcrette, M.; Edstroem, K.; Jumas, J. C.; Tarascon, J. M. *J. Mater. Chem.* **2007**, *17*, 3759−3772.
(9) Yang, J.; Takeda, Y.; Imanishi, N.; Yamamoto, O. *J. Electrochem. Soc.* **1999**, *146*, 4009−4013.
(10) Wang, C.; Zhou, Y.; Ge, M. Y.; Xu, X. B.; Zhang, Z. L.; Jiang, J. Z. *J. Am. Chem. Soc.* **2010**, *132*, 46−47.
(11) Wang, Y.; Lee, J. Y.; Zeng, H. C. *Chem. Mater.* **2005**, *17*, 3899−3903.
(12) Guo, Z. P.; Du, G. D.; Nuli, Y.; Hassanb, M. F.; Liu, H. K. *J. Mater. Chem.* **2009**, *19*, 3253−3257.
(13) Park, M. S.; Wang, G. X.; Kang, Y. M.; Wexler, D.; Dou, S. X.; Liu, H. K. *Angew. Chem., Int. Ed.* **2007**, *46*, 750−753.
(14) Zhao, N. H.; Wang, G. J.; Huang, Y.; Wang, B.; Yao, B. D.; Wu, Y. P. *Chem. Mater.* **2008**, *20*, 2612−2614.
(15) Wang, C.; Zhou, Y.; Ge, M. Y.; Xu, X. B.; Zhang, Z. L.; Jiang, J. Z. *J. Am. Chem. Soc.* **2010**, *132*, 46−47.
(16) Kim, J. G.; Nam, S. H.; Lee, S. H.; Choi, S. M.; Kim, W. B. *ACS Appl. Mater. Interfaces* **2011**, *3*, 828−835.
(17) Lou, X. W.; Chen, J. S.; Chen, P.; Archer, L. A. *Chem. Mater.* **2009**, *21*, 2868−2874.
(18) Yang, R.; Zhao, W.; Zheng, J.; Zhang, X. Z.; Li, X. G. *J. Phys. Chem. C* **2010**, *114*, 20272−20276.
(19) Lou, X. W.; Li, C. M.; Archer, A. L. *Adv. Mater.* **2009**, *21*, 2536−2539.
(20) Yuan, L.; Konstantinov, K.; Wang, G. X.; Liu, H. K.; Dou, S. X. *J. Power Sources* **2005**, *146*, 180−184.
(21) Novoselov, K. S.; Geim, A. K.; Morozov, S. V.; Jiang, D.; Zhang, Y.; Dubonos, S. V.; Grigorieva, I. V.; Firsov, A. A. *Science* **2004**, *306*, 666−669.
(22) Geim, A. K.; Novoselov, K. S. *Nat. Mater.* **2007**, *6*, 183−191.
(23) Geim, A. K. *Science* **2009**, *324*, 1530−1534.
(24) Stankovich, S.; Dikin, D. A.; Piner, R. D.; Kohlhaas, K. A.; Kleinhammes, A.; Jia, Y.; Wu, Y.; Nguyen, S. T.; Ruoff, R. S. *Carbon* **2007**, *45*, 1558−1565.
(25) Li, D.; Muller, M. B.; Gilje, S.; Kaner, R. B.; Wallace, G. G. *Nat. Nanotechnol.* **2008**, *3*, 101−105.
(26) Williams, G.; Seger, B.; Kamat, P. V. *ACS Nano* **2008**, *2*, 1487−1491.
(27) Liu, J. B.; Fu, S. H.; Yuan, B.; Li, Y. L.; Deng, Z. X. *J. Am. Chem. Soc.* **2010**, *132*, 7279−7281.
(28) Cao, A. N.; Liu, Z.; Chu, S. S.; Wu, M. H.; Ye, Z. M.; Cai, Z. W.; Chang, Y. L.; Wang, S. F.; Gong, Q. H.; Liu, Y. F. *Adv. Mater.* **2010**, *22*, 103−106.
(29) Bunker, B. C.; Rieke, P. C.; Tarasevich, B. J.; Campbell, A. A.; Fryxell, G. E.; Graff, G. L.; Song, L.; Liu, J.; Virden, J. W.; McVay, G. L. *Science* **1994**, *264*, 48−55.
(30) Paek, S. M.; Yoo, E.; Honma, I. *Nano Lett.* **2009**, *9*, 72−75.
(31) Wang, D. H.; Kou, R.; Choi, D.; Yang, Z. G.; Nie, Z. M.; Li, J.; Saraf, L. V.; Hu, D. H.; Zhang, J. G.; Graff, G. L.; Liu, J.; Pope, M. A.; Aksay, I. A. *ACS Nano* **2010**, *4*, 1587−1595.
(32) Zhang, L. S.; Jiang, L. Y.; Yan, H. J.; Wang, W. D.; Wang, W.; Song, W. G.; Guo, Y. G.; Wan, L. J. *J. Mater. Chem.* **2010**, *20*, 5462−5467.
(33) Wang, Z. Y.; Zhang, H.; Li, N.; Shi, Z. J.; Gu, Z. N.; Cao, G. P. *Nano Res.* **2010**, *3*, 748−756.
(34) Kim, H.; Kim, S. W.; Park, Y. U.; Gwon, H.; Seo, D. H.; Kim, Y.; Kang, K. *Nano Res.* **2010**, *3*, 813−821.
(35) Yao, J.; Shen, X. P.; Wang, B.; Liu, H. K.; Wang, G. X. *Electrochem. Commun.* **2009**, *11*, 1849−1852.
(36) Du, Z. F.; Yin, X. M.; Zhang, M.; Hao, Q. Y.; Wang, Y. G.; Wang, T. H. *Mater. Lett.* **2010**, *64*, 2076−2079.
(37) Li, F. H.; Song, J. F.; Yang, H. F.; Gan, S. Y.; Zhang, Q. X.; Han, D. X.; Ivaska, A.; Niu, L. *Nanotechnology* **2009**, *20*, 455602.
(38) Li, Y. M.; Lv, X. J.; Lu, J.; Li, J. H. *J. Phys. Chem. C* **2010**, *114*, 21770−21774.
(39) Zhang, J. T.; Xiong, Z. G.; Zhao, X. S. *J. Mater. Chem.* **2011**, *21*, 3634−3640.
(40) Zhang, M.; Lei, D. N.; Du, Z. F.; Yin, X. M.; Chen, L. B.; Li, Q. H.; Wang, Y. G.; Wang, T. H. *J. Mater. Chem.* **2011**, *21*, 1673−1676.
(41) Wang, X. Y.; Zhou, X. F.; Yao, K.; Zhang, J. G.; Liu, Z. P. *Carbon* **2011**, *49*, 133−139.
(42) Kovtyukhova, N. I.; Ollivier, P. J.; Martin, B. R.; Mallouk, T. E.; Chizhik, S. A.; Buzaneva, E. V.; Gorchinskiy, A. D. *Chem. Mater.* **1999**, *11*, 771−778.
(43) Stankovich, S.; Dikin, D. A.; Dommett, G. H. B.; Kohlhaas, K. M.; Zimney, E. Z.; Stach, E. A.; Piner, R. D.; Nguyen, S. T.; Ruoff, R. S. *Nature* **2006**, *442*, 282−286.
(44) Zhong, L. S.; Hu, J. S.; Cui, Z. M.; Wan, L. J.; Song, W. G. *Chem. Mater.* **2007**, *19*, 4557−4562.
(45) Lian, P. C.; Zhu, X. F.; Liang, S. Z.; Li, Z.; Yang, W. S.; Wang, H. H. *Electrochim. Acta* **2011**, *56*, 4532−4539.
(46) Meng, X. B.; Geng, D. S.; Liu, J. A.; Banis, M. N.; Zhang, Y.; Li, R. Y.; Sun, X. L. *J. Phys. Chem. C* **2010**, *114*, 18330−18337.
(47) He, Y. B.; Tang, Z. Y.; Song, Q. S.; Xie, H.; Liu, Y. G.; Xu, Q. *J. Electrochem. Soc.* **2008**, *7*, A481−A487.